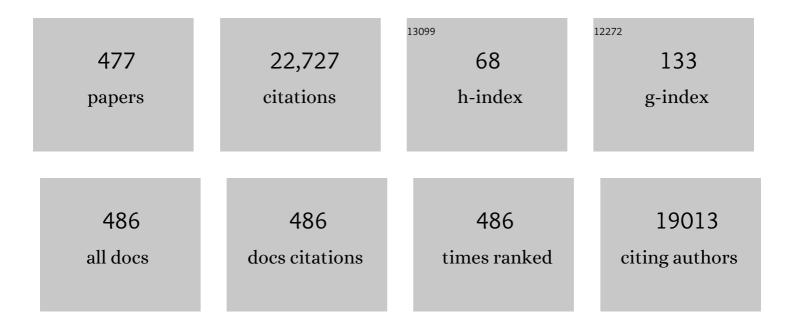
List of Publications by Year in descending order

Source: https://exaly.com/author-pdf/5143816/publications.pdf Version: 2024-02-01



ANANT MADARHUSHI

#	Article	IF	CITATIONS
1	Histopathological Image Analysis: A Review. IEEE Reviews in Biomedical Engineering, 2009, 2, 147-171.	18.0	1,511
2	Applications of machine learning in drug discovery and development. Nature Reviews Drug Discovery, 2019, 18, 463-477.	46.4	1,358
3	Deep learning for digital pathology image analysis: A comprehensive tutorial with selected use cases. Journal of Pathology Informatics, 2016, 7, 29.	1.7	850
4	Artificial intelligence in digital pathology — new tools for diagnosis and precision oncology. Nature Reviews Clinical Oncology, 2019, 16, 703-715.	27.6	807
5	Image analysis and machine learning in digital pathology: Challenges and opportunities. Medical Image Analysis, 2016, 33, 170-175.	11.6	670
6	Stacked Sparse Autoencoder (SSAE) for Nuclei Detection on Breast Cancer Histopathology Images. IEEE Transactions on Medical Imaging, 2016, 35, 119-130.	8.9	659
7	Evaluation of prostate segmentation algorithms for MRI: The PROMISE12 challenge. Medical Image Analysis, 2014, 18, 359-373.	11.6	469
8	Intratumoral and peritumoral radiomics for the pretreatment prediction of pathological complete response to neoadjuvant chemotherapy based on breast DCE-MRI. Breast Cancer Research, 2017, 19, 57.	5.0	408
9	A Deep Convolutional Neural Network for segmenting and classifying epithelial and stromal regions in histopathological images. Neurocomputing, 2016, 191, 214-223.	5.9	365
10	Radiomics and radiogenomics in lung cancer: A review for the clinician. Lung Cancer, 2018, 115, 34-41.	2.0	362
11	Accurate and reproducible invasive breast cancer detection in whole-slide images: A Deep Learning approach for quantifying tumor extent. Scientific Reports, 2017, 7, 46450.	3.3	360
12	Digital Imaging in Pathology: Whole-Slide Imaging and Beyond. Annual Review of Pathology: Mechanisms of Disease, 2013, 8, 331-359.	22.4	355
13	A Review of Deep Learning in Medical Imaging: Imaging Traits, Technology Trends, Case Studies With Progress Highlights, and Future Promises. Proceedings of the IEEE, 2021, 109, 820-838.	21.3	339
14	Assessment of algorithms for mitosis detection in breast cancer histopathology images. Medical Image Analysis, 2015, 20, 237-248.	11.6	338
15	Mitosis detection in breast cancer pathology images by combining handcrafted and convolutional neural network features. Journal of Medical Imaging, 2014, 1, 034003.	1.5	264
16	Combining low-, high-level and empirical domain knowledge for automated segmentation of ultrasonic breast lesions. IEEE Transactions on Medical Imaging, 2003, 22, 155-169.	8.9	248
17	Computerized Image-Based Detection and Grading of Lymphocytic Infiltration in HER2+ Breast Cancer Histopathology. IEEE Transactions on Biomedical Engineering, 2010, 57, 642-653.	4.2	229
18	Perinodular and Intranodular Radiomic Features on Lung CT Images Distinguish Adenocarcinomas from Granulomas. Radiology, 2019, 290, 783-792.	7.3	226

#	Article	IF	CITATIONS
19	Automatic detection of invasive ductal carcinoma in whole slide images with convolutional neural networks. Proceedings of SPIE, 2014, , .	0.8	224
20	Predicting cancer outcomes with radiomics and artificial intelligence in radiology. Nature Reviews Clinical Oncology, 2022, 19, 132-146.	27.6	221
21	Radiomic features from the peritumoral brain parenchyma on treatment-naÃ ⁻ ve multi-parametric MR imaging predict long versus short-term survival in glioblastoma multiforme: Preliminary findings. European Radiology, 2017, 27, 4188-4197.	4.5	210
22	A Boosted Bayesian Multiresolution Classifier for Prostate Cancer Detection From Digitized Needle Biopsies. IEEE Transactions on Biomedical Engineering, 2012, 59, 1205-1218.	4.2	209
23	A Deep Learning Architecture for Image Representation, Visual Interpretability and Automated Basal-Cell Carcinoma Cancer Detection. Lecture Notes in Computer Science, 2013, 16, 403-410.	1.3	209
24	Identification of a MicroRNA Panel for Clear-cell Kidney Cancer. Urology, 2010, 75, 835-841.	1.0	208
25	An Integrated Region-, Boundary-, Shape-Based Active Contour for Multiple Object Overlap Resolution in Histological Imagery. IEEE Transactions on Medical Imaging, 2012, 31, 1448-1460.	8.9	205
26	Association of Peritumoral Radiomics With Tumor Biology and Pathologic Response to Preoperative Targeted Therapy for <i>HER2 (ERBB2)</i> –Positive Breast Cancer. JAMA Network Open, 2019, 2, e192561.	5.9	196
27	Changes in CT Radiomic Features Associated with Lymphocyte Distribution Predict Overall Survival and Response to Immunotherapy in Non–Small Cell Lung Cancer. Cancer Immunology Research, 2020, 8, 108-119.	3.4	187
28	Automated gland and nuclei segmentation for grading of prostate and breast cancer histopathology. , 2008, , .		183
29	Expectation–Maximization-Driven Geodesic Active Contour With Overlap Resolution (EMaGACOR): Application to Lymphocyte Segmentation on Breast Cancer Histopathology. IEEE Transactions on Biomedical Engineering, 2010, 57, 1676-1689.	4.2	171
30	Spatial Architecture and Arrangement of Tumor-Infiltrating Lymphocytes for Predicting Likelihood of Recurrence in Early-Stage Non–Small Cell Lung Cancer. Clinical Cancer Research, 2019, 25, 1526-1534.	7.0	168
31	HistoQC: An Open-Source Quality Control Tool for Digital Pathology Slides. JCO Clinical Cancer Informatics, 2019, 3, 1-7.	2.1	167
32	Digital pathology image analysis: opportunities and challenges. Imaging in Medicine, 2009, 1, 7-10.	0.0	165
33	Automated detection of prostatic adenocarcinoma from high-resolution ex vivo MRI. IEEE Transactions on Medical Imaging, 2005, 24, 1611-1625.	8.9	164
34	Stain Normalization using Sparse AutoEncoders (StaNoSA): Application to digital pathology. Computerized Medical Imaging and Graphics, 2017, 57, 50-61.	5.8	161
35	Digital pathology and computational image analysis in nephropathology. Nature Reviews Nephrology, 2020, 16, 669-685.	9.6	133
36	AUTOMATED GRADING OF PROSTATE CANCER USING ARCHITECTURAL AND TEXTURAL IMAGE FEATURES. , 2007, , .		128

ANANT MADABHUSHI

#	Article	IF	CITATIONS
37	Automated grading of breast cancer histopathology using spectral clusteringwith textural and architectural image features. , 2008, , .		128
38	Computerized Image Analysis for Identifying Triple-Negative Breast Cancers and Differentiating Them from Other Molecular Subtypes of Breast Cancer on Dynamic Contrast-enhanced MR Images: A Feasibility Study. Radiology, 2014, 272, 91-99.	7.3	127
39	Emerging Themes in Image Informatics and Molecular Analysis for Digital Pathology. Annual Review of Biomedical Engineering, 2016, 18, 387-412.	12.3	117
40	New methods of MR image intensity standardization via generalized scale. Medical Physics, 2006, 33, 3426-3434.	3.0	116
41	Radiomic features for prostate cancer detection on MRI differ between the transition and peripheral zones: Preliminary findings from a multiâ€institutional study. Journal of Magnetic Resonance Imaging, 2017, 46, 184-193.	3.4	114
42	Radiogenomic analysis of hypoxia pathway is predictive of overall survival in Glioblastoma. Scientific Reports, 2018, 8, 7.	3.3	113
43	Central gland and peripheral zone prostate tumors have significantly different quantitative imaging signatures on 3 tesla endorectal, in vivo T2â€weighted MR imagery. Journal of Magnetic Resonance Imaging, 2012, 36, 213-224.	3.4	112
44	Multifeature Landmark-Free Active Appearance Models: Application to Prostate MRI Segmentation. IEEE Transactions on Medical Imaging, 2012, 31, 1638-1650.	8.9	110
45	High-throughput detection of prostate cancer in histological sections using probabilistic pairwise Markov models. Medical Image Analysis, 2010, 14, 617-629.	11.6	107
46	Radiomic features from pretreatment biparametric MRI predict prostate cancer biochemical recurrence: Preliminary findings. Journal of Magnetic Resonance Imaging, 2018, 48, 1626-1636.	3.4	107
47	Pitfalls in assessing stromal tumor infiltrating lymphocytes (sTILs) in breast cancer. Npj Breast Cancer, 2020, 6, 17.	5.2	106
48	Computer-aided prognosis: Predicting patient and disease outcome via quantitative fusion of multi-scale, multi-modal data. Computerized Medical Imaging and Graphics, 2011, 35, 506-514.	5.8	104
49	Textural Kinetics: A Novel Dynamic Contrast-Enhanced (DCE)-MRI Feature for Breast Lesion Classification. Journal of Digital Imaging, 2011, 24, 446-463.	2.9	104
50	Multi-Field-of-View Framework for Distinguishing Tumor Grade in ER+ Breast Cancer From Entire Histopathology Slides. IEEE Transactions on Biomedical Engineering, 2013, 60, 2089-2099.	4.2	104
51	Co-occurrence of Local Anisotropic Gradient Orientations (CoLlAGe): A new radiomics descriptor. Scientific Reports, 2016, 6, 37241.	3.3	104
52	Development and evaluation of deep learning–based segmentation of histologic structures in the kidney cortex with multiple histologic stains. Kidney International, 2021, 99, 86-101.	5.2	103
53	Interplay between intensity standardization and inhomogeneity correction in MR image processing. IEEE Transactions on Medical Imaging, 2005, 24, 561-576.	8.9	100
54	Elastic registration of multimodal prostate MRI and histology via multiattribute combined mutual information. Medical Physics, 2011, 38, 2005-2018.	3.0	100

#	Article	IF	CITATIONS
55	High-throughput adaptive sampling for whole-slide histopathology image analysis (HASHI) via convolutional neural networks: Application to invasive breast cancer detection. PLoS ONE, 2018, 13, e0196828.	2.5	100
56	Nuclear shape and orientation features from H&E images predict survival in early-stage estrogen receptor-positive breast cancers. Laboratory Investigation, 2018, 98, 1438-1448.	3.7	99
57	Artificial Intelligence and Machine Learning in Arrhythmias and Cardiac Electrophysiology. Circulation: Arrhythmia and Electrophysiology, 2020, 13, e007952.	4.8	96
58	Computer-Extracted Texture Features to Distinguish Cerebral Radionecrosis from Recurrent Brain Tumors on Multiparametric MRI: A Feasibility Study. American Journal of Neuroradiology, 2016, 37, 2231-2236.	2.4	95
59	Radiomics Analysis on FLT-PET/MRI for Characterization of Early Treatment Response in Renal Cell Carcinoma: A Proof-of-Concept Study. Translational Oncology, 2016, 9, 155-162.	3.7	94
60	A deep-learning classifier identifies patients with clinical heart failure using whole-slide images of H&E tissue. PLoS ONE, 2018, 13, e0192726.	2.5	93
61	Investigating the Efficacy of Nonlinear Dimensionality Reduction Schemes in Classifying Gene and Protein Expression Studies. IEEE/ACM Transactions on Computational Biology and Bioinformatics, 2008, 5, 368-384.	3.0	91
62	Report on computational assessment of Tumor Infiltrating Lymphocytes from the International Immuno-Oncology Biomarker Working Group. Npj Breast Cancer, 2020, 6, 16.	5.2	90
63	Radiomic features on MRI enable risk categorization of prostate cancer patients on active surveillance: Preliminary findings. Journal of Magnetic Resonance Imaging, 2018, 48, 818-828.	3.4	88
64	Multi-kernel graph embedding for detection, Gleason grading of prostate cancer via MRI/MRS. Medical Image Analysis, 2013, 17, 219-235.	11.6	85
65	Prediction of recurrence in early stage non-small cell lung cancer using computer extracted nuclear features from digital H&E images. Scientific Reports, 2017, 7, 13543.	3.3	85
66	CT derived radiomic score for predicting the added benefit of adjuvant chemotherapy following surgery in stage I, II resectable non-small cell lung cancer: a retrospective multicohort study for outcome prediction. The Lancet Digital Health, 2020, 2, e116-e128.	12.3	85
67	Supervised Multi-View Canonical Correlation Analysis (sMVCCA): Integrating Histologic and Proteomic Features for Predicting Recurrent Prostate Cancer. IEEE Transactions on Medical Imaging, 2015, 34, 284-297.	8.9	82
68	Cascaded discrimination of normal, abnormal, and confounder classes in histopathology: Gleason grading of prostate cancer. BMC Bioinformatics, 2012, 13, 282.	2.6	81
69	Machine Learning Prediction of Response to Cardiac Resynchronization Therapy. Circulation: Arrhythmia and Electrophysiology, 2019, 12, e007316.	4.8	76
70	Harnessing non-destructive 3D pathology. Nature Biomedical Engineering, 2021, 5, 203-218.	22.5	74
71	A Quantitative Histomorphometric Classifier (QuHbIC) Identifies Aggressive Versus Indolent p16-Positive Oropharyngeal Squamous Cell Carcinoma. American Journal of Surgical Pathology, 2014, 38, 128-137.	3.7	73
72	Combination of Peri- and Intratumoral Radiomic Features on Baseline CT Scans Predicts Response to Chemotherapy in Lung Adenocarcinoma. Radiology: Artificial Intelligence, 2019, 1, 180012.	5.8	73

#	Article	IF	CITATIONS
73	Automated Tubule Nuclei Quantification and Correlation with Oncotype DX risk categories in ER+ Breast Cancer Whole Slide Images. Scientific Reports, 2016, 6, 32706.	3.3	72
74	Quality control stress test for deep learning-based diagnostic model in digital pathology. Modern Pathology, 2021, 34, 2098-2108.	5.5	72
75	NCI Workshop Report: Clinical and Computational Requirements for Correlating Imaging Phenotypes with Genomics Signatures. Translational Oncology, 2014, 7, 556-569.	3.7	69
76	Radiomics based targeted radiotherapy planning (Rad-TRaP): a computational framework for prostate cancer treatment planning with MRI. Radiation Oncology, 2016, 11, 148.	2.7	69
77	Quantitative nuclear histomorphometry predicts oncotype DX risk categories for early stage ER+ breast cancer. BMC Cancer, 2018, 18, 610.	2.6	67
78	Radiogenomic-Based Survival Risk Stratification of Tumor Habitat on Gd-T1w MRI Is Associated with Biological Processes in Glioblastoma. Clinical Cancer Research, 2020, 26, 1866-1876.	7.0	67
79	Novel, non-invasive imaging approach to identify patients with advanced non-small cell lung cancer at risk of hyperprogressive disease with immune checkpoint blockade. , 2020, 8, e001343.		64
80	A Boosting Cascade for Automated Detection of Prostate Cancer from Digitized Histology. Lecture Notes in Computer Science, 2006, 9, 504-511.	1.3	63
81	Computer aided diagnostic tools aim to empower rather than replace pathologists: Lessons learned from computational chess. Journal of Pathology Informatics, 2011, 2, 25.	1.7	62
82	Determining histology-MRI slice correspondences for defining MRI-based disease signatures of prostate cancer. Computerized Medical Imaging and Graphics, 2011, 35, 568-578.	5.8	61
83	Shape Features of the Lesion Habitat to Differentiate Brain Tumor Progression from Pseudoprogression on Routine Multiparametric MRI: A Multisite Study. American Journal of Neuroradiology, 2018, 39, 2187-2193.	2.4	61
84	An active learning based classification strategy for the minority class problem: application to histopathology annotation. BMC Bioinformatics, 2011, 12, 424.	2.6	60
85	Multimodal wavelet embedding representation for data combination (MaWERiC): integrating magnetic resonance imaging and spectroscopy for prostate cancer detection. NMR in Biomedicine, 2012, 25, 607-619.	2.8	60
86	An oral cavity squamous cell carcinoma quantitative histomorphometric-based image classifier of nuclear morphology can risk stratify patients for disease-specific survival. Modern Pathology, 2017, 30, 1655-1665.	5.5	60
87	An integrated nomogram combining deep learning, Prostate Imaging–Reporting and Data System (PI-RADS) scoring, and clinical variables for identification of clinically significant prostate cancer on biparametric MRI: a retrospective multicentre study. The Lancet Digital Health, 2021, 3, e445-e454.	12.3	55
88	Generalized scale: Theory, algorithms, and application to image inhomogeneity correction. Computer Vision and Image Understanding, 2006, 101, 100-121.	4.7	54
89	Sparse Non-negative Matrix Factorization (SNMF) based color unmixing for breast histopathological image analysis. Computerized Medical Imaging and Graphics, 2015, 46, 20-29.	5.8	54
90	Evaluating stability of histomorphometric features across scanner and staining variations: prostate cancer diagnosis from whole slide images. Journal of Medical Imaging, 2016, 3, 047502.	1.5	54

#	Article	IF	CITATIONS
91	A deep learning based strategy for identifying and associating mitotic activity with gene expression derived risk categories in estrogen receptor positive breast cancers. Cytometry Part A: the Journal of the International Society for Analytical Cytology, 2017, 91, 566-573.	1.5	54
92	Co-Occurring Gland Angularity in Localized Subgraphs: Predicting Biochemical Recurrence in Intermediate-Risk Prostate Cancer Patients. PLoS ONE, 2014, 9, e97954.	2.5	53
93	Novel Quantitative Imaging for Predicting Response to Therapy: Techniques and Clinical Applications. American Society of Clinical Oncology Educational Book / ASCO American Society of Clinical Oncology Meeting, 2018, 38, 1008-1018.	3.8	52
94	Predicting pathologic response to neoadjuvant chemoradiation in resectable stage III non-small cell lung cancer patients using computed tomography radiomic features. Lung Cancer, 2019, 135, 1-9.	2.0	51
95	An Image Analysis Resource for Cancer Research: PIIP—Pathology Image Informatics Platform for Visualization, Analysis, and Management. Cancer Research, 2017, 77, e83-e86.	0.9	50
96	Radiomic Features of Primary Rectal Cancers on Baseline T ₂ â€Weighted MRI Are Associated With Pathologic Complete Response to Neoadjuvant Chemoradiation: A Multisite Study. Journal of Magnetic Resonance Imaging, 2020, 52, 1531-1541.	3.4	50
97	A Radio-genomics Approach for Identifying High Risk Estrogen Receptor-positive Breast Cancers on DCE-MRI: Preliminary Results in Predicting OncotypeDX Risk Scores. Scientific Reports, 2016, 6, 21394.	3.3	49
98	Quantitative Image Analysis of Human Epidermal Growth Factor Receptor 2 Immunohistochemistry for Breast Cancer: Guideline From the College of American Pathologists. Archives of Pathology and Laboratory Medicine, 2019, 143, 1180-1195.	2.5	49
99	Combination of Peri-Tumoral and Intra-Tumoral Radiomic Features on Bi-Parametric MRI Accurately Stratifies Prostate Cancer Risk: A Multi-Site Study. Cancers, 2020, 12, 2200.	3.7	49
100	Role of tumor infiltrating lymphocytes and spatial immune heterogeneity in sensitivity to PD-1 axis blockers in non-small cell lung cancer. , 2022, 10, e004440.		49
101	A high-throughput active contour scheme for segmentation of histopathological imagery. Medical Image Analysis, 2011, 15, 851-862.	11.6	48
102	A hierarchical spectral clustering and nonlinear dimensionality reduction scheme for detection of prostate cancer from magnetic resonance spectroscopy (MRS). Medical Physics, 2009, 36, 3927-3939.	3.0	46
103	Nuclear Shape and Architecture in Benign Fields Predict Biochemical Recurrence in Prostate Cancer Patients Following Radical Prostatectomy: Preliminary Findings. European Urology Focus, 2017, 3, 457-466.	3.1	46
104	Accurate Prostate Volume Estimation Using Multifeature Active Shape Models on T2-weighted MRI. Academic Radiology, 2011, 18, 745-754.	2.5	44
105	Identifying the morphologic basis for radiomic features in distinguishing different Gleason grades of prostate cancer on MRI: Preliminary findings. PLoS ONE, 2018, 13, e0200730.	2.5	44
106	Computer-extracted Features Can Distinguish Noncancerous Confounding Disease from Prostatic Adenocarcinoma at Multiparametric MR Imaging. Radiology, 2016, 278, 135-145.	7.3	43
107	Prostate Cancer Risk Stratification via Nondestructive 3D Pathology with Deep Learning–Assisted Gland Analysis. Cancer Research, 2022, 82, 334-345.	0.9	42
108	A magnetic resonance spectroscopy driven initialization scheme for active shape model based prostate segmentation. Medical Image Analysis, 2011, 15, 214-225.	11.6	41

#	Article	IF	CITATIONS
109	Multi-field-of-view strategy for image-based outcome prediction of multi-parametric estrogen receptor-positive breast cancer histopathology: Comparison to Oncotype DX. Journal of Pathology Informatics, 2012, 2, 1.	1.7	40
110	Explicit shape descriptors: Novel morphologic features for histopathology classification. Medical Image Analysis, 2013, 17, 997-1009.	11.6	40
111	A prognostic model for overall survival of patients with early-stage non-small cell lung cancer: a multicentre, retrospective study. The Lancet Digital Health, 2020, 2, e594-e606.	12.3	38
112	An integrated segmentation and shape-based classification scheme for distinguishing adenocarcinomas from granulomas on lung CT. Medical Physics, 2017, 44, 3556-3569.	3.0	37
113	A resolution adaptive deep hierarchical (RADHicaL) learning scheme applied to nuclear segmentation of digital pathology images. Computer Methods in Biomechanics and Biomedical Engineering: Imaging and Visualization, 2018, 6, 270-276.	1.9	37
114	Incorporating domain knowledge for tubule detection in breast histopathology using O'Callaghan neighborhoods. Proceedings of SPIE, 2011, , .	0.8	36
115	Computationally Derived Image Signature of Stromal Morphology Is Prognostic of Prostate Cancer Recurrence Following Prostatectomy in African American Patients. Clinical Cancer Research, 2020, 26, 1915-1923.	7.0	36
116	An automated computational image analysis pipeline for histological grading of cardiac allograft rejection. European Heart Journal, 2021, 42, 2356-2369.	2.2	36
117	Cell Orientation Entropy (COrE): Predicting Biochemical Recurrence from Prostate Cancer Tissue Microarrays. Lecture Notes in Computer Science, 2013, 16, 396-403.	1.3	36
118	Supervised Regularized Canonical Correlation Analysis: integrating histologic and proteomic measurements for predicting biochemical recurrence following prostate surgery. BMC Bioinformatics, 2011, 12, 483.	2.6	34
119	HistoStitcher©: An interactive program for accurate and rapid reconstruction of digitized whole histological sections from tissue fragments. Computerized Medical Imaging and Graphics, 2011, 35, 557-567.	5.8	34
120	Cell cluster graph for prediction of biochemical recurrence in prostate cancer patients from tissue microarrays. Proceedings of SPIE, 2013, , .	0.8	34
121	Comparing radiomic classifiers and classifier ensembles for detection of peripheral zone prostate tumors on T2-weighted MRI: a multi-site study. BMC Medical Imaging, 2019, 19, 22.	2.7	34
122	Feature-driven local cell graph (FLocK): New computational pathology-based descriptors for prognosis of lung cancer and HPV status of oropharyngeal cancers. Medical Image Analysis, 2021, 68, 101903.	11.6	34
123	Simultaneous segmentation of prostatic zones using Active Appearance Models with multiple coupled levelsets. Computer Vision and Image Understanding, 2013, 117, 1051-1060.	4.7	33
124	Towards Improved Cancer Diagnosis and Prognosis Using Analysis of Gene Expression Data and Computer Aided Imaging. Experimental Biology and Medicine, 2009, 234, 860-879.	2.4	32
125	A novel imaging based Nomogram for predicting post-surgical biochemical recurrence and adverse pathology of prostate cancer from pre-operative bi-parametric MRI. EBioMedicine, 2021, 63, 103163.	6.1	32
126	A deep learning classifier for prediction of pathological complete response to neoadjuvant		32

chemotherapy from baseline breast DCE-MRI., 2018, , .

#	Article	IF	CITATIONS
127	Integrated diagnostics: a conceptual framework with examples. Clinical Chemistry and Laboratory Medicine, 2010, 48, 989-998.	2.3	31
128	Statistical shape model for manifold regularization: Gleason grading of prostate histology. Computer Vision and Image Understanding, 2013, 117, 1138-1146.	4.7	31
129	EM-based segmentation-driven color standardization of digitized histopathology. Proceedings of SPIE, 2013, , .	0.8	31
130	Cascaded ensemble of convolutional neural networks and handcrafted features for mitosis detection. Proceedings of SPIE, 2014, , .	0.8	31
131	The state of the art for artificial intelligence in lung digital pathology. Journal of Pathology, 2022, 257, 413-429.	4.5	31
132	Spatial interplay patterns of cancer nuclei and tumor-infiltrating lymphocytes (TILs) predict clinical benefit for immune checkpoint inhibitors. Science Advances, 2022, 8, .	10.3	31
133	Decision Support System for Detection of Diabetic Retinopathy Using Smartphones. , 2013, , .		30
134	Multisite evaluation of radiomic feature reproducibility and discriminability for identifying peripheral zone prostate tumors on MRI. Journal of Medical Imaging, 2019, 6, 1.	1.5	30
135	High-Throughput Biomarker Segmentation on Ovarian Cancer Tissue Microarrays via Hierarchical Normalized Cuts. IEEE Transactions on Biomedical Engineering, 2012, 59, 1240-1252.	4.2	29
136	Technical Note: MRQy — An openâ€source tool for quality control of MR imaging data. Medical Physics, 2020, 47, 6029-6038.	3.0	29
137	Machine Learning of 12-Lead QRS Waveforms to Identify Cardiac Resynchronization Therapy Patients With Differential Outcomes. Circulation: Arrhythmia and Electrophysiology, 2020, 13, e008210.	4.8	29
138	Stable and discriminating radiomic predictor of recurrence in early stage non-small cell lung cancer: Multi-site study. Lung Cancer, 2020, 142, 90-97.	2.0	29
139	Artificial intelligence applied to breast pathology. Virchows Archiv Fur Pathologische Anatomie Und Physiologie Und Fur Klinische Medizin, 2022, 480, 191-209.	2.8	29
140	Detecting Prostatic Adenocarcinoma From Digitized Histology Using a Multi-Scale Hierarchical Classification Approach. , 2006, 2006, 4759-62.		28
141	Selective invocation of shape priors for deformable segmentation and morphologic classification of prostate cancer tissue microarrays. Computerized Medical Imaging and Graphics, 2015, 41, 3-13.	5.8	28
142	Integrating structural and functional imaging for computer assisted detection of prostate cancer on multi-protocol in vivo 3 Tesla MRI. Proceedings of SPIE, 2009, 7260, 72603I.	0.8	27
143	Concurrent segmentation of the prostate on MRI and CT via linked statistical shape models for radiotherapy planning. Medical Physics, 2012, 39, 2214-2228.	3.0	27
144	Novel PCA-VIP scheme for ranking MRI protocols and identifying computer-extracted MRI measurements associated with central gland and peripheral zone prostate tumors. Journal of Magnetic Resonance Imaging, 2015, 41, 1383-1393.	3.4	27

#	Article	IF	CITATIONS
145	Identifying in vivo DCE MRI markers associated with microvessel architecture and gleason grades of prostate cancer. Journal of Magnetic Resonance Imaging, 2016, 43, 149-158.	3.4	27
146	Stable and discriminating features are predictive of cancer presence and Gleason grade in radical prostatectomy specimens: a multi-site study. Scientific Reports, 2018, 8, 14918.	3.3	27
147	CT-Radiomic Approach to Predict G1/2 Nonfunctional Pancreatic Neuroendocrine Tumor. Academic Radiology, 2020, 27, e272-e281.	2.5	27
148	Machine Learning–Derived Fractal Features of Shape and Texture of the Left Atrium and Pulmonary Veins From Cardiac Computed Tomography Scans Are Associated With Risk of Recurrence of Atrial Fibrillation Postablation. Circulation: Arrhythmia and Electrophysiology, 2021, 14, e009265.	4.8	27
149	A Comprehensive Segmentation, Registration, and Cancer Detection Scheme on 3 Tesla In Vivo Prostate DCE-MRI. Lecture Notes in Computer Science, 2008, 11, 662-669.	1.3	26
150	Collagen fiber orientation disorder from H&E images is prognostic for early stage breast cancer: clinical trial validation. Npj Breast Cancer, 2021, 7, 104.	5.2	26
151	Tumor Habitat–derived Radiomic Features at Pretreatment MRI That Are Prognostic for Progression-free Survival in Glioblastoma Are Associated with Key Morphologic Attributes at Histopathologic Examination: A Feasibility Study. Radiology: Artificial Intelligence, 2020, 2, e190168.	5.8	26
152	Novel imaging biomarkers predict outcomes in stage III unresectable non-small cell lung cancer treated with chemoradiation and durvalumab. , 2022, 10, e003778.		26
153	Class-specific weighting for Markov random field estimation: Application to medical image segmentation. Medical Image Analysis, 2012, 16, 1477-1489.	11.6	25
154	Multi-Pass Adaptive Voting for Nuclei Detection in Histopathological Images. Scientific Reports, 2016, 6, 33985.	3.3	25
155	Assessment of a computerized quantitative quality control tool for whole slide images of kidney biopsies. Journal of Pathology, 2021, 253, 268-278.	4.5	25
156	A weighted mean shift, normalized cuts initialized color gradient based geodesic active contour model: applications to histopathology image segmentation. Proceedings of SPIE, 2010, , .	0.8	24
157	Feature Importance in Nonlinear Embeddings (FINE): Applications in Digital Pathology. IEEE Transactions on Medical Imaging, 2016, 35, 76-88.	8.9	24
158	Radiomic Texture and Shape Descriptors of the Rectal Environment on Post-Chemoradiation T2-Weighted MRI are Associated with Pathologic Tumor Stage Regression in Rectal Cancers: A Retrospective, Multi-Institution Study. Cancers, 2020, 12, 2027.	3.7	24
159	Sexually dimorphic radiogenomic models identify distinct imaging and biological pathways that are prognostic of overall survival in glioblastoma. Neuro-Oncology, 2021, 23, 251-263.	1.2	24
160	T1 and T2 MR fingerprinting measurements of prostate cancer and prostatitis correlate with deep learning–derived estimates of epithelium, lumen, and stromal composition on corresponding whole mount histopathology. European Radiology, 2021, 31, 1336-1346.	4.5	24
161	Computerized tumor multinucleation index (MuNI) is prognostic in p16+ oropharyngeal carcinoma. Journal of Clinical Investigation, 2021, 131, .	8.2	24
162	Quantitative vessel tortuosity: A potential CT imaging biomarker for distinguishing lung granulomas from adenocarcinomas. Scientific Reports, 2018, 8, 15290.	3.3	23

#	Article	IF	CITATIONS
163	Correlation between MRI phenotypes and a genomic classifier of prostate cancer: preliminary findings. European Radiology, 2019, 29, 4861-4870.	4.5	23
164	Repeatability of radiomics and machine learning for DWI: Shortâ€ŧerm repeatability study of 112 patients with prostate cancer. Magnetic Resonance in Medicine, 2020, 83, 2293-2309.	3.0	23
165	Adaptive Energy Selective Active Contour with Shape Priors for Nuclear Segmentation and Gleason Grading of Prostate Cancer. Lecture Notes in Computer Science, 2011, 14, 661-669.	1.3	23
166	An Imaging Biomarker of Tumor-Infiltrating Lymphocytes to Risk-Stratify Patients With HPV-Associated Oropharyngeal Cancer. Journal of the National Cancer Institute, 2022, 114, 609-617.	6.3	23
167	Comparing MR image intensity standardization against tissue characterizability of magnetization transfer ratio imaging. Journal of Magnetic Resonance Imaging, 2006, 24, 667-675.	3.4	22
168	Spectral embedding based active contour (SEAC) for lesion segmentation on breast dynamic contrast enhanced magnetic resonance imaging. Medical Physics, 2013, 40, 032305.	3.0	22
169	Computerized spermatogenesis staging (CSS) of mouse testis sections via quantitative histomorphological analysis. Medical Image Analysis, 2021, 70, 101835.	11.6	22
170	Graph Embedding to Improve Supervised Classification and Novel Class Detection: Application to Prostate Cancer. Lecture Notes in Computer Science, 2005, 8, 729-737.	1.3	22
171	Spatially Aware Cell Cluster(SpACCl) Graphs: Predicting Outcome in Oropharyngeal p16+ Tumors. Lecture Notes in Computer Science, 2013, 16, 412-419.	1.3	22
172	Content-based image retrieval of digitized histopathology in boosted spectrally embedded spaces. Journal of Pathology Informatics, 2015, 6, 41.	1.7	22
173	Advanced Morphologic Analysis for Diagnosing Allograft Rejection. Transplantation, 2018, 102, 1230-1239.	1.0	21
174	Image Segmentation with Implicit Color Standardization Using Spatially Constrained Expectation Maximization: Detection of Nuclei. Lecture Notes in Computer Science, 2012, 15, 365-372.	1.3	21
175	Empirical evaluation of cross-site reproducibility in radiomic features for characterizing prostate MRI. , 2018, , .		21
176	Computer-aided prognosis of ER+ breast cancer histopathology and correlating survival outcome with Oncotype DX assay. , 2009, , .		20
177	A knowledge representation framework for integration, classification of multi-scale imaging and non-imaging data: Preliminary results in predicting prostate cancer recurrence by fusing mass spectrometry and histology. , 2009, , .		20
178	Multi-modal data fusion schemes for integrated classification of imaging and non-imaging biomedical data. , 2011, 2011, 165-168.		20
179	An integrated texton and bag of words classifier for identifying anaplastic medulloblastomas. , 2011, 2011, 3443-6.		20
180	Automated Computer-derived Prostate Volumes from MR Imaging Data: Comparison with Radiologist-derived MR Imaging and Pathologic Specimen Volumes. Radiology, 2012, 262, 144-151.	7.3	20

#	Article	IF	CITATIONS
181	Texture descriptors to distinguish radiation necrosis from recurrent brain tumors on multi-parametric MRI. , 2014, 9035, 90352B.		20
182	A method for medulloblastoma tumor differentiation based on convolutional neural networks and transfer learning. Proceedings of SPIE, 2015, , .	0.8	20
183	Co-registration of pre-operative CT with ex vivo surgically excised ground glass nodules to define spatial extent of invasive adenocarcinoma on in vivo imaging: a proof-of-concept study. European Radiology, 2017, 27, 4209-4217.	4.5	20
184	Combination of computer extracted shape and texture features enables discrimination of granulomas from adenocarcinoma on chest computed tomography. Journal of Medical Imaging, 2018, 5, 1.	1.5	20
185	Image analysis reveals molecularly distinct patterns of TILs in NSCLC associated with treatment outcome. Npj Precision Oncology, 2022, 6, .	5.4	20
186	A multi-modal prostate segmentation scheme by combining spectral clustering and active shape models. , 2008, , .		19
187	Evaluating feature selection strategies for high dimensional, small sample size datasets. , 2011, 2011, 949-52.		19
188	Cascaded Multi-view Canonical Correlation (CaMCCo) for Early Diagnosis of Alzheimer's Disease via Fusion of Clinical, Imaging and Omic Features. Scientific Reports, 2017, 7, 8137.	3.3	19
189	Single cell qPCR reveals that additional HAND2 and microRNA-1 facilitate the early reprogramming progress of seven-factor-induced human myocytes. PLoS ONE, 2017, 12, e0183000.	2.5	19
190	Markov Random Field driven Region-Based Active Contour Model (MaRACel): Application to Medical Image Segmentation. Lecture Notes in Computer Science, 2010, 13, 197-204.	1.3	19
191	Using head movement to recognize activity. , 0, , .		18
192	Spatially weighted mutual information (SWMI) for registration of digitally reconstructed ex vivo whole mount histology and in vivo prostate MRI. , 2011, 2011, 6269-72.		18
193	Histostitcherâ"¢: An informatics software platform for reconstructing whole-mount prostate histology using the extensible imaging platform framework. Journal of Pathology Informatics, 2014, 5, 8.	1.7	18
194	Out-of-Sample Extrapolation utilizing Semi-Supervised Manifold Learning (OSE-SSL): Content Based Image Retrieval for Histopathology Images. Scientific Reports, 2016, 6, 27306.	3.3	18
195	Co-Registration of ex vivo Surgical Histopathology and in vivo T2 weighted MRI of the Prostate via multi-scale spectral embedding representation. Scientific Reports, 2017, 7, 8717.	3.3	18
196	Distinguishing granulomas from adenocarcinomas by integrating stable and discriminating radiomic features on non-contrast computed tomography scans. European Journal of Cancer, 2021, 148, 146-158.	2.8	18
197	Semi Supervised Multi Kernel (SeSMiK) Graph Embedding: Identifying Aggressive Prostate Cancer via Magnetic Resonance Imaging and Spectroscopy. Lecture Notes in Computer Science, 2010, 13, 666-673.	1.3	18
198	Interplay between bias field correction, intensity standardization, and noise filtering for T2-weighted MRI. , 2011, 2011, 5080-3.		17

12

#	Article	IF	CITATIONS
199	Identifying quantitative in vivo multi-parametric MRI features for treatment related changes after laser interstitial thermal therapy of prostate cancer. Neurocomputing, 2014, 144, 13-23.	5.9	17
200	Dimensionality reduction-based fusion approaches for imaging and non-imaging biomedical data: concepts, workflow, and use-cases. BMC Medical Imaging, 2017, 17, 2.	2.7	17
201	Deep Learning Tissue Segmentation in Cardiac Histopathology Images. , 2017, , 179-195.		17
202	Quantitative nuclear histomorphometric features are predictive of Oncotype DX risk categories in ductal carcinoma in situ: preliminary findings. Breast Cancer Research, 2019, 21, 114.	5.0	17
203	Computer Extracted Features from Initial H&E Tissue Biopsies Predict Disease Progression for Prostate Cancer Patients on Active Surveillance. Cancers, 2020, 12, 2708.	3.7	17
204	Quantitative Assessment of the Effects of Compression on Deep Learning in Digital Pathology Image Analysis. JCO Clinical Cancer Informatics, 2020, 4, 221-233.	2.1	17
205	A new machine learning approach for predicting likelihood of recurrence following ablation for atrial fibrillation from CT. BMC Medical Imaging, 2021, 21, 45.	2.7	17
206	A Pathologist-Annotated Dataset for Validating Artificial Intelligence: A Project Description and Pilot Study. Journal of Pathology Informatics, 2021, 12, 45.	1.7	17
207	Enhanced multi-protocol analysis via intelligent supervised embedding (EMPrAvISE): detecting prostate cancer on multi-parametric MRI. Proceedings of SPIE, 2011, 7963, 79630U.	0.8	16
208	Briefâ€exposure to preoperative bevacizumab reveals a TGFâ€Î² signature predictive of response in HER2â€negative breast cancers. International Journal of Cancer, 2016, 138, 747-757.	5.1	16
209	Mass Effect Deformation Heterogeneity (MEDH) on Gadolinium-contrast T1-weighted MRI is associated with decreased survival in patients with right cerebral hemisphere Glioblastoma: A feasibility study. Scientific Reports, 2019, 9, 1145.	3.3	16
210	Deep-learning approaches for Gleason grading of prostate biopsies. Lancet Oncology, The, 2020, 21, 187-189.	10.7	16
211	Radiomic Features Associated With HPV Status on Pretreatment Computed Tomography in Oropharyngeal Squamous Cell Carcinoma Inform Clinical Prognosis. Frontiers in Oncology, 2021, 11, 744250.	2.8	16
212	Co-occurrence of Local Anisotropic Gradient Orientations (CoLlAGe): Distinguishing Tumor Confounders and Molecular Subtypes on MRI. Lecture Notes in Computer Science, 2014, 17, 73-80.	1.3	16
213	Convolutional neural network initialized active contour model with adaptive ellipse fitting for nuclear segmentation on breast histopathological images. Journal of Medical Imaging, 2019, 6, 1.	1.5	16
214	Oropharyngeal cancer outcomes correlate with p16 status, multinucleation and immune infiltration. Modern Pathology, 2022, 35, 1045-1054.	5.5	16
215	Fully automated prostate magnetic resonance imaging and transrectal ultrasound fusion via a probabilistic registration metric. , 2013, 8671, .		15
216	Identifying MRI Markers Associated with Early Response following Laser Ablation for Neurological Disorders: Preliminary Findings. PLoS ONE, 2014, 9, e114293.	2.5	15

#	Article	IF	CITATIONS
217	Advances in the computational and molecular understanding of the prostate cancer cell nucleus. Journal of Cellular Biochemistry, 2018, 119, 7127-7142.	2.6	15
218	Radiomics-based assessment of ultra-widefield leakage patterns and vessel network architecture in the PERMEATE study: insights into treatment durability. British Journal of Ophthalmology, 2021, 105, 1155-1160.	3.9	15
219	Test-retest repeatability of a deep learning architecture in detecting and segmenting clinically significant prostate cancer on apparent diffusion coefficient (ADC) maps. European Radiology, 2021, 31, 379-391.	4.5	15
220	Quick Annotator: an openâ€source digital pathology based rapid image annotation tool. Journal of Pathology: Clinical Research, 2021, 7, 542-547.	3.0	15
221	Computationally Derived Cribriform Area Index from Prostate Cancer Hematoxylin and Eosin Images Is Associated with Biochemical Recurrence Following Radical Prostatectomy and Is Most Prognostic in Gleason Grade Group 2. European Urology Focus, 2021, 7, 722-732.	3.1	15
222	Novel Non-Invasive Radiomic Signature on CT Scans Predicts Response to Platinum-Based Chemotherapy and Is Prognostic of Overall Survival in Small Cell Lung Cancer. Frontiers in Oncology, 2021, 11, 744724.	2.8	15
223	A Novel Stochastic Combination of 3D Texture Features for Automated Segmentation of Prostatic Adenocarcinoma from High Resolution MRI. Lecture Notes in Computer Science, 2003, , 581-591.	1.3	14
224	Distinguishing Lesions from Posterior Acoustic Shadowing in Breast Ultrasound via Non-Linear Dimensionality Reduction. , 2006, 2006, 3070-3.		14
225	Cascaded multi-class pairwise classifier (CascaMPa) for normal, cancerous, and cancer confounder classes in prostate histology. , 2011, , .		14
226	Quantifying local heterogeneity via morphologic scale: Distinguishing tumoral from stromal regions. Journal of Pathology Informatics, 2013, 4, 8.	1.7	14
227	Spatio-temporal texture (SpTeT) for distinguishing vulnerable from stable atherosclerotic plaque on dynamic contrast enhancement (DCE) MRI in a rabbit model. Medical Physics, 2014, 41, 042303.	3.0	14
228	Framework for 3D histologic reconstruction and fusion with in vivo MRI: Preliminary results of characterizing pulmonary inflammation in a mouse model. Medical Physics, 2015, 42, 4822-4832.	3.0	14
229	Imaging Features of Vessels and Leakage Patterns Predict Extended Interval Aflibercept Dosing Using Ultra-Widefield Angiography in Retinal Vascular Disease: Findings From the PERMEATE Study. IEEE Transactions on Biomedical Engineering, 2021, 68, 1777-1786.	4.2	14
230	A Visual Latent Semantic Approach for Automatic Analysis and Interpretation of Anaplastic Medulloblastoma Virtual Slides. Lecture Notes in Computer Science, 2012, 15, 157-164.	1.3	14
231	Quantitative Imaging Biomarkers in Age-Related Macular Degeneration and Diabetic Eye Disease: A Step Closer to Precision Medicine. Journal of Personalized Medicine, 2021, 11, 1161.	2.5	14
232	Artificial intelligence and melanoma: A comprehensive review of clinical, dermoscopic, and histologic applications. Pigment Cell and Melanoma Research, 2022, 35, 203-211.	3.3	14
233	Multimodal image registration of ex vivo 4 Tesla MRI with whole mount histology for prostate cancer detection. , 2007, , .		13
234	Image filtering via generalized scale. Medical Image Analysis, 2008, 12, 87-98.	11.6	13

ANANT MADABHUSHI

#	Article	IF	CITATIONS
235	Active Contour for Overlap Resolution using Watershed BASED initialization (ACOReW): Applications to histopathology. , 2011, , .		13
236	Consensus embedding: theory, algorithms and application to segmentation and classification of biomedical data. BMC Bioinformatics, 2012, 13, 26.	2.6	13
237	Computer extracted gland features from H&E predicts prostate cancer recurrence comparably to a genomic companion diagnostic test: a large multi-site study. Npj Precision Oncology, 2021, 5, 35.	5.4	13
238	Integrated Clinical and CT Based Artificial Intelligence Nomogram for Predicting Severity and Need for Ventilator Support in COVID-19 Patients: A Multi-Site Study. IEEE Journal of Biomedical and Health Informatics, 2021, 25, 4110-4118.	6.3	13
239	An Empirical Comparison of Dimensionality Reduction Methods for Classifying Gene and Protein Expression Datasets. , 2007, , 170-181.		13
240	A Hierarchical Unsupervised Spectral Clustering Scheme for Detection of Prostate Cancer from Magnetic Resonance Spectroscopy (MRS). , 2007, 10, 278-286.		13
241	Pattern Recognition in Histopathological Images: An ICPR 2010 Contest. Lecture Notes in Computer Science, 2010, , 226-234.	1.3	13
242	A COMBINED FEATURE ENSEMBLE BASED MUTUAL INFORMATION SCHEME FOR ROBUST INTER-MODAL, INTER-PROTOCOL IMAGE REGISTRATION. , 2007, , .		12
243	A boosted distance metric: application to content based image retrieval and classification of digitized histopathology. Proceedings of SPIE, 2009, , .	0.8	12
244	Evaluation of effects of JPEC2000 compression on a computer-aided detection system for prostate cancer on digitized histopathology. , 2010, , .		12
245	Multiattribute probabilistic prostate elastic registration (MAPPER): Application to fusion of ultrasound and magnetic resonance imaging. Medical Physics, 2015, 42, 1153-1163.	3.0	12
246	Breast Cancer Diagnosis Using Neural-Based Linear Fusion Strategies. Lecture Notes in Computer Science, 2006, , 165-175.	1.3	12
247	Combining Unsupervised Feature Learning and Riesz Wavelets for Histopathology Image Representation: Application to Identifying Anaplastic Medulloblastoma. Lecture Notes in Computer Science, 2015, , 581-588.	1.3	12
248	Novel Morphometric Based Classification via Diffeomorphic Based Shape Representation Using Manifold Learning. Lecture Notes in Computer Science, 2010, 13, 658-665.	1.3	12
249	Radiomics-based convolutional neural network for brain tumor segmentation on multiparametric magnetic resonance imaging. Journal of Medical Imaging, 2019, 6, 1.	1.5	12
250	A quantitative exploration of efficacy of gland morphology in prostate cancer grading. , 2007, , .		11
251	Segmentation and classification of triple negative breast cancers using DCE-MRI. , 2009, , .		11
252	Predicting classifier performance with a small training set: Applications to computer-aided diagnosis and prognosis. , 2010, , .		11

#	Article	IF	CITATIONS
253	Integration of Architectural and Cytologic Driven Image Algorithms for Prostate Adenocarcinoma Identification. Analytical Cellular Pathology, 2012, 35, 251-265.	1.4	11
254	Optimization of Complex Cancer Morphology Detection Using the SIVQ Pattern Recognition Algorithm. Analytical Cellular Pathology, 2012, 35, 41-50.	1.4	11
255	Quantitative identification of magnetic resonance imaging features of prostate cancer response following laser ablation and radical prostatectomy. Journal of Medical Imaging, 2014, 1, 035001.	1.5	11
256	Distinguishing prostate cancer from benign confounders via a cascaded classifier on multi-parametric MRI. Proceedings of SPIE, 2014, , .	0.8	11
257	Prostate shapes on pre-treatment MRI between prostate cancer patients who do and do not undergo biochemical recurrence are different: Preliminary Findings. Scientific Reports, 2017, 7, 15829.	3.3	11
258	A prognostic and predictive computational pathology image signature for added benefit of adjuvant chemotherapy in early stage non-small-cell lung cancer. EBioMedicine, 2021, 69, 103481.	6.1	11
259	Hierarchical Normalized Cuts: Unsupervised Segmentation of Vascular Biomarkers from Ovarian Cancer Tissue Microarrays. Lecture Notes in Computer Science, 2009, 12, 230-238.	1.3	11
260	Computer-extracted features relating to spatial arrangement of tumor infiltrating lymphocytes to predict response to nivolumab in non-small cell lung cancer (NSCLC) Journal of Clinical Oncology, 2018, 36, 12115-12115.	1.6	11
261	Detection of prostate cancer on histopathology using color fractals and Probabilistic Pairwise Markov models. , 2011, 2011, 3427-30.		10
262	Prostatome: A combined anatomical and disease based MRI atlas of the prostate. Medical Physics, 2014, 41, 072301.	3.0	10
263	Computational imaging reveals shape differences between normal and malignant prostates on MRI. Scientific Reports, 2017, 7, 41261.	3.3	10
264	Coregistration of Preoperative MRI with Ex Vivo Mesorectal Pathology Specimens to Spatially Map Post-treatment Changes in Rectal Cancer Onto In Vivo Imaging. Academic Radiology, 2018, 25, 833-841.	2.5	10
265	Feature Driven Local Cell Graph (FeDeG): Predicting Overall Survival in Early Stage Lung Cancer. Lecture Notes in Computer Science, 2018, , 407-416.	1.3	10
266	Disorder in Pixel-Level Edge Directions on T1WI Is Associated with the Degree of Radiation Necrosis in Primary and Metastatic Brain Tumors: Preliminary Findings. American Journal of Neuroradiology, 2019, 40, 412-417.	2.4	10
267	Reimagining T Staging Through Artificial Intelligence and Machine Learning Image Processing Approaches in Digital Pathology. JCO Clinical Cancer Informatics, 2020, 4, 1039-1050.	2.1	10
268	Automated gleason grading on prostate biopsy slides by statistical representations of homology profile. Computer Methods and Programs in Biomedicine, 2020, 194, 105528.	4.7	10
269	Prospective Evaluation of Repeatability and Robustness of Radiomic Descriptors in Healthy Brain Tissue Regions In Vivo Across Systematic Variations in <scp>T2</scp> â€Weighted Magnetic Resonance Imaging Acquisition Parameters. Journal of Magnetic Resonance Imaging, 2021, 54, 1009-1021.	3.4	10
270	Consensus-Locally Linear Embedding (C-LLE): Application to Prostate Cancer Detection on Magnetic Resonance Spectroscopy. Lecture Notes in Computer Science, 2008, 11, 330-338.	1.3	10

#	Article	IF	CITATIONS
271	High-Throughput Prostate Cancer Gland Detection, Segmentation, and Classification from Digitized Needle Core Biopsies. Lecture Notes in Computer Science, 2010, , 77-88.	1.3	10
272	Computer extracted features of cancer nuclei from H&E stained tissues of tumor predicts response to nivolumab in non-small cell lung cancer Journal of Clinical Oncology, 2018, 36, 12061-12061.	1.6	10
273	Image microarrays (IMA): Digital pathology′s missing tool. Journal of Pathology Informatics, 2011, 2, 47.	1.7	10
274	Computer-Aided Laser Dissection: A Microdissection Workflow Leveraging Image Analysis Tools. Journal of Pathology Informatics, 2018, 9, 45.	1.7	10
275	Computational image features of immune architecture is associated with clinical benefit and survival in gynecological cancers across treatment modalities. , 2022, 10, e003833.		10
276	COLLINARUS: collection of image-derived non-linear attributes for registration using splines. , 2009, , .		9
277	Empirical evaluation of bias field correction algorithms for computer-aided detection of prostate cancer on T2w MRI. , 2011, , .		9
278	Predicting Classifier Performance with Limited Training Data: Applications to Computer-Aided Diagnosis in Breast and Prostate Cancer. PLoS ONE, 2015, 10, e0117900.	2.5	9
279	Comparing Ensembles of Learners: Detecting Prostate Cancer from High Resolution MRI. Lecture Notes in Computer Science, 2006, , 25-36.	1.3	9
280	Response Estimation Through Spatially Oriented Neural Network and Texture Ensemble (RESONATE). Lecture Notes in Computer Science, 2019, , 602-610.	1.3	9
281	Optimization of complex cancer morphology detection using the SIVQ pattern recognition algorithm. Analytical Cellular Pathology, 2012, 35, 41-50.	1.4	9
282	Automatic boundary extraction of ultrasonic breast lesions. , 0, , .		8
283	Multi-Compartment Spatially-Derived Radiomics From Optical Coherence Tomography Predict Anti-VEGF Treatment Durability in Macular Edema Secondary to Retinal Vascular Disease: Preliminary Findings. IEEE Journal of Translational Engineering in Health and Medicine, 2021, 9, 1-13.	3.7	8
284	Spectral Embedding Based Probabilistic Boosting Tree (ScEPTre): Classifying High Dimensional Heterogeneous Biomedical Data. Lecture Notes in Computer Science, 2009, 12, 844-851.	1.3	8
285	Quantitative vessel tortuosity radiomics on baseline non-contrast lung CT predict response to immunotherapy and are prognostic of overall survival. , 2019, , .		8
286	Prostate Surface Distension and Tumor Texture Descriptors From Pre-Treatment MRI Are Associated With Biochemical Recurrence Following Radical Prostatectomy: Preliminary Findings. Frontiers in Oncology, 0, 12, .	2.8	8
287	Improving supervised classification accuracy using non-rigid multimodal image registration: detecting prostate cancer. , 2008, , .		7
288	A consensus embedding approach for segmentation of high resolution in vivo prostate magnetic resonance imagery. Proceedings of SPIE, 2008, , .	0.8	7

ANANT MADABHUSHI

#	Article	IF	CITATIONS
289	Segmenting multiple overlapping objects via a hybrid active contour model incorporating shape priors: applications to digital pathology. Proceedings of SPIE, 2011, , .	0.8	7
290	A comparative evaluation of supervised and unsupervised representation learning approaches for anaplastic medulloblastoma differentiation. , 2015, , .		7
291	AutoStitcher: An Automated Program for Efficient and Robust Reconstruction of Digitized Whole Histological Sections from Tissue Fragments. Scientific Reports, 2016, 6, 29906.	3.3	7
292	Tu1966 A Machine-Learning Based Risk Score to Predict Response to Therapy in Crohn's Disease via Baseline MRE. Gastroenterology, 2016, 150, S992.	1.3	7
293	Radiogenomic analysis of hypoxia pathway reveals computerized MRI descriptors predictive of overall survival in glioblastoma. Proceedings of SPIE, 2017, , .	0.8	7
294	Training a cell-level classifier for detecting basal-cell carcinoma by combining human visual attention maps with low-level handcrafted features. Journal of Medical Imaging, 2017, 4, 021105.	1.5	7
295	Image-based risk score to predict recurrence of ER+ breast cancer in ECOG-ACRIN Cancer Research Group E2197 Journal of Clinical Oncology, 2018, 36, 540-540.	1.6	7
296	Variable Importance in Nonlinear Kernels (VINK): Classification of Digitized Histopathology. Lecture Notes in Computer Science, 2013, 16, 238-245.	1.3	7
297	Radiographic-Deformation and Textural Heterogeneity (r-DepTH): An Integrated Descriptor for Brain Tumor Prognosis. Lecture Notes in Computer Science, 2017, , 459-467.	1.3	7
298	Multi-tissue Partitioning for Whole Slide Images of Colorectal Cancer Histopathology Images with Deeptissue Net. Lecture Notes in Computer Science, 2019, , 100-108.	1.3	7
299	Survival prediction on intrahepatic cholangiocarcinoma with histomorphological analysis on the whole slide images. Computers in Biology and Medicine, 2022, 146, 105520.	7.0	7
300	Expectation Maximization driven Geodesic Active Contour with Overlap Resolution (EMaGACOR): Application to Lymphocyte Segmentation on Breast Cancer Histopathology. , 2009, , .		6
301	A boosted classifier for integrating multiple fields of view: Breast cancer grading in histopathology. , 2011, , .		6
302	Supervised regularized canonical correlation analysis: Integrating histologic and proteomic data for predicting biochemical failures. , 2011, 2011, 6434-7.		6
303	Variable Ranking with PCA: Finding Multiparametric MR Imaging Markers for Prostate Cancer Diagnosis and Grading. Lecture Notes in Computer Science, 2011, , 146-157.	1.3	6
304	CADOnc ⓒ: An integrated toolkit for evaluating radiation therapy related changes in the prostate using multiparametric MRI. , 2011, 2011, 2095-2098.		6
305	Weighted Maximum Posterior Marginals for Random Fields Using an Ensemble of Conditional Densities From Multiple Markov Chain Monte Carlo Simulations. IEEE Transactions on Medical Imaging, 2011, 30, 1353-1364.	8.9	6
306	Segmentation of nodular medulloblastoma using Random Walker and Hierarchical Normalized Cuts. ,		6

2011,,.

#	Article	IF	CITATIONS
307	Gleason grading of prostate histology utilizing manifold regularization via statistical shape model of manifolds. , 2012, , .		6
308	Quantitative evaluation of treatment related changes on multi-parametric MRI after laser interstitial thermal therapy of prostate cancer. Proceedings of SPIE, 2013, 8671, 86711F.	0.8	6
309	Quantitative evaluation of multi-parametric MR imaging marker changes post-laser interstitial ablation therapy (LITT) for epilepsy. Proceedings of SPIE, 2013, 8671, 86711Y.	0.8	6
310	Supervised multi-view canonical correlation analysis: fused multimodal prediction of disease diagnosis and prognosis. Proceedings of SPIE, 2014, , .	0.8	6
311	Vascular Network Organization via Hough Transform (VaNgOGH): A Novel Radiomic Biomarker for Diagnosis andÂTreatment Response. Lecture Notes in Computer Science, 2018, , 803-811.	1.3	6
312	Semi-Supervised Graph Embedding Scheme with Active Learning (SSGEAL): Classifying High Dimensional Biomedical Data. Lecture Notes in Computer Science, 2010, , 207-218.	1.3	6
313	RaPtomics: integrating radiomic and pathomic features for predicting recurrence in early stage lung cancer. , 2018, , .		6
314	Correlation of radiomic features with PD-L1 expression in early stage non-small cell lung cancer (ES-NSCLC) to predict recurrence and overall survival (OS) Journal of Clinical Oncology, 2018, 36, e24247-e24247.	1.6	6
315	Quantifying Post- Laser Ablation Prostate Therapy Changes on MRI via a Domain-Specific Biomechanical Model: Preliminary Findings. PLoS ONE, 2016, 11, e0150016.	2.5	6
316	Integration of architectural and cytologic driven image algorithms for prostate adenocarcinoma identification. Analytical Cellular Pathology, 2012, 35, 251-65.	1.4	6
317	Novel Radiomic Measurements of Tumor-Associated Vasculature Morphology on Clinical Imaging as a Biomarker of Treatment Response in Multiple Cancers. Clinical Cancer Research, 2022, 28, 4410-4424.	7.0	6
318	A machine learning model for separating epithelial and stromal regions in oral cavity squamous cell carcinomas using H&E-stained histology images: A multi-center, retrospective study. Oral Oncology, 2022, 131, 105942.	1.5	6
319	Probabilistic pairwise Markov models: application to prostate cancer detection. Proceedings of SPIE, 2009, , .	0.8	5
320	Graphical processing unit implementation of an integrated shape-based active contour: Application to digital pathology. Journal of Pathology Informatics, 2011, 2, 13.	1.7	5
321	Statistical 3D prostate imaging atlas construction via anatomically constrained registration. , 2013, 8669, .		5
322	Anisotropic smoothing regularization (AnSR) in Thirion's Demons registration evaluates brain MRI tissue changes post-laser ablation. , 2013, 2013, 4006-9.		5
323	Computer extracted texture features on T2w MRI to predict biochemical recurrence following radiation therapy for prostate cancer. Proceedings of SPIE, 2014, , .	0.8	5
324	A learning based fiducial-driven registration scheme for evaluating laser ablation changes in neurological disorders. Neurocomputing, 2014, 144, 24-37.	5.9	5

#	Article	IF	CITATIONS
325	A domain constrained deformable (DoCD) model for co-registration of pre- and post-radiated prostate MRI. Neurocomputing, 2014, 144, 3-12.	5.9	5
326	A note on the stability and discriminability of graph-based features for classification problems in digital pathology. , 2015, , .		5
327	Automated tubule nuclei quantification and correlation with oncotype DX risk categories in ER+ breast cancer whole slide images. , 2016, , .		5
328	Optical High Content Nanoscopy of Epigenetic Marks Decodes Phenotypic Divergence in Stem Cells. Scientific Reports, 2017, 7, 39406.	3.3	5
329	Radiomic features from pretreatment biparametric MRI predict prostate cancer biochemical recurrence: Preliminary findings. Journal of Magnetic Resonance Imaging, 2018, 48, spcone-spcone.	3.4	5
330	Impact of p16 Status and Anatomical Site in Anti-PD-1 Immunotherapy-Treated Recurrent/Metastatic Head and Neck Squamous Cell Carcinoma Patients. Cancers, 2021, 13, 4861.	3.7	5
331	Multi-Attribute Non-initializing Texture Reconstruction Based Active Shape Model (MANTRA). Lecture Notes in Computer Science, 2008, 11, 653-661.	1.3	5
332	Consensus of Ambiguity: Theory and Application of Active Learning for Biomedical Image Analysis. Lecture Notes in Computer Science, 2010, , 313-324.	1.3	5
333	Changes in computer extracted features of vessel tortuosity on CT scans post-treatment in responders compared to non-responders for non-small cell lung cancer on immunotherapy Journal of Clinical Oncology, 2017, 35, 11518-11518.	1.6	5
334	Development and external validation of a deep learning model for predicting response to HER2-targeted neoadjuvant therapy from pretreatment breast MRI Journal of Clinical Oncology, 2019, 37, 593-593.	1.6	5
335	OCT-Derived Radiomic Features Predict Anti–VEGF Response and Durability in Neovascular Age-Related Macular Degeneration. Ophthalmology Science, 2022, 2, 100171.	2.5	5
336	Generalized scale: theory, algorithms, and application to image inhomogeneity correction. , 2004, , .		4
337	A structural-functional MRI-based disease atlas: application to computer-aided-diagnosis of prostate cancer. Proceedings of SPIE, 2010, , .	0.8	4
338	Multi-attribute combined mutual information (MACMI): An image registration framework for leveraging multiple data channels. , 2010, , .		4
339	Computer-aided prognosis: Predicting patient and disease outcome via multi-modal image analysis. , 2010, , .		4
340	Spectral embedding based active contour (SEAC): application to breast lesion segmentation on DCE-MRI. Proceedings of SPIE, 2011, , .	0.8	4
341	A texture-based classifier to discriminate anaplastic from non-anaplastic medulloblastoma. , 2011, , .		4
342	Integrating an adaptive region-based appearance model with a landmark-free statistical shape model: application to prostate MRI segmentation. , 2011, , .		4

#	Article	IF	CITATIONS
343	A statistical deformation model (SDM) based regularizer for non-rigid image registration: application to registration of multimodal prostate MRI and histology. , 2013, , .		4
344	Connecting Markov random fields and active contour models: application to gland segmentation and classification. Journal of Medical Imaging, 2017, 4, 021107.	1.5	4
345	A Novel Nodule Edge Sharpness Radiomic Biomarker Improves Performance of Lung-RADS for Distinguishing Adenocarcinomas from Granulomas on Non-Contrast CT Scans. Cancers, 2021, 13, 2781.	3.7	4
346	Computational pathology reveals unique spatial patterns of immune response in H&E images from COVID-19 autopsies: preliminary findings. Journal of Medical Imaging, 2021, 8, 017501.	1.5	4
347	Characterization of Ultra-Widefield Angiographic Vascular Features in Diabetic Retinopathy with Automated Severity Classification. Ophthalmology Science, 2021, 1, 100049.	2.5	4
348	Weighted Combination of Multi-Parametric MR Imaging Markers for Evaluating Radiation Therapy Related Changes in the Prostate. Lecture Notes in Computer Science, 2011, , 80-91.	1.3	4
349	A combination of intra- and peritumoral features on baseline CT scans is associated with overall survival in non-small cell lung cancer patients treated with immune checkpoint inhibitors: a multi-agent multi-site study. , 2019, , .		4
350	Computerized textural analysis of lung CT to enable quantification of tumor infiltrating lymphocytes in NSCLC Journal of Clinical Oncology, 2016, 34, 11584-11584.	1.6	4
351	Evolution of radiomic features on serial CT scans as an imaging based biomarker for evaluating response in patients with non-small cell lung cancer treated with nivolumab Journal of Clinical Oncology, 2017, 35, e14534-e14534.	1.6	4
352	Histopathological Image Analysis on Mouse Testes for Automated Staging of Mouse Seminiferous Tubule. Lecture Notes in Computer Science, 2019, , 117-124.	1.3	4
353	Computerâ€extracted features of nuclear morphology in hematoxylin and eosin images distinguish <scp>s</scp> tage <scp>II</scp> and <scp>IV</scp> colon tumors. Journal of Pathology, 2022, 257, 17-28.	4.5	4
354	Evaluating intensity standardization and inhomogeneity correction in magnetic resonance images. , 0,		3
355	Novel kinetic texture features for breast lesion classification on dynamic contrast enhanced (DCE) MRI. , 2008, , .		3
356	Local morphologic scale: application to segmenting tumor infiltrating lymphocytes in ovarian cancer TMAs. Proceedings of SPIE, 2011, , .	0.8	3
357	Image segmentation with implicit color standardization using cascaded EM: Detection of myelodysplastic syndromes. , 2012, , .		3
358	Co-occurring gland tensors in localized cluster graphs: Quantitative histomorphometry for predicting biochemical recurrence for intermediate grade prostate cancer. , 2013, , .		3
359	Multiscale multimodal fusion of histological and MRI volumes for characterization of lung inflammation. Proceedings of SPIE, 2013, , .	0.8	3
360	Identifying in vivo DCE MRI parameters correlated with ex vivo quantitative microvessel architecture: A radiohistomorphometric approach. , 2013, , .		3

#	Article	IF	CITATIONS
361	Identifying MRI markers to evaluate early treatment-related changes post-laser ablation for cancer pain management. , 2014, 9036, 90362L.		3
362	Computerized Histologic Image Based Risk Predictor (CHIRP): Identifying Disease Aggressiveness Using Sub-visual Image Cues from Image Data. Microscopy and Microanalysis, 2016, 22, 1006-1007.	0.4	3
363	Patient-specific pharmacokinetic parameter estimation on dynamic contrast-enhanced MRI of prostate: Preliminary evaluation of a novel AIF-free estimation method. Journal of Magnetic Resonance Imaging, 2016, 44, 1405-1414.	3.4	3
364	Evaluating stability of histomorphometric features across scanner and staining variations: predicting biochemical recurrence from prostate cancer whole slide images. , 2016, , .		3
365	Discriminative Scale Learning (DiScrn): Applications to Prostate Cancer Detection from MRI and Needle Biopsies. Scientific Reports, 2017, 7, 12375.	3.3	3
366	RADIomic Spatial TexturAl descripTor (RADISTAT): Characterizing Intra-tumoral Heterogeneity for Response and Outcome Prediction. Lecture Notes in Computer Science, 2017, , 468-476.	1.3	3
367	Novel imaging biomarkers predict progression-free survival in stage 3 NSCLC treated with chemoradiation and durvalumab Journal of Clinical Oncology, 2021, 39, 3054-3054.	1.6	3
368	Intra-perinodular Textural Transition (Ipris): A 3D Descriptor for Nodule Diagnosis on Lung CT. Lecture Notes in Computer Science, 2017, , 647-655.	1.3	3
369	Evaluation of radiomic features on baseline CT scan to predict clinical benefit for pemetrexed based chemotherapy in metastatic lung adenocarcinoma Journal of Clinical Oncology, 2016, 34, 11582-11582.	1.6	3
370	Computer-extracted stromal features of African-Americans versus Caucasians from H&E slides and impact on prognosis of biochemical recurrence Journal of Clinical Oncology, 2018, 36, 12075-12075.	1.6	3
371	Adaptive Dimensionality Reduction with Semi-Supervision (AdDReSS): Classifying Multi-Attribute Biomedical Data. PLoS ONE, 2016, 11, e0159088.	2.5	3
372	A watershed and feature-based approach for automated detection of lymphocytes on lung cancer images. , 2018, , .		3
373	RADIomic Spatial TexturAl Descriptor (RADISTAT): Quantifying Spatial Organization of Imaging Heterogeneity Associated With Tumor Response to Treatment. IEEE Journal of Biomedical and Health Informatics, 2022, 26, 2627-2636.	6.3	3
374	Machine Learning to Predict Risk of Relapse Using Cytologic Image Markers in Patients With Acute Myeloid Leukemia Posthematopoietic Cell Transplantation. JCO Clinical Cancer Informatics, 2022, 6, e2100156.	2.1	3
375	New methods of MR image intensity standardization via generalized scale. , 2005, , .		2
376	Generalized scale-based image filtering. , 2005, , .		2
377	WERITAS: weighted ensemble of regional image textures for ASM segmentation. , 2009, , .		2
378	Content-based image retrieval utilizing explicit shape descriptors: applications to breast MRI and prostate histopathology. Proceedings of SPIE, 2011, , .	0.8	2

#	Article	IF	CITATIONS
379	MP60-04 QUANTITATIVE ASSESSMENT OF T2-WEIGHTED MRI TO BETTER IDENTIFY PATIENTS WITH PROSTATE CANCER IN A SCREENING POPULATION. Journal of Urology, 2015, 193, .	0.4	2
380	Multi-modality registration via multi-scale textural and spectral embedding representations. , 2016, , .		2
381	Editorial Comment. Urology, 2016, 88, 132-133.	1.0	2
382	Special Section Guest Editorial: Digital Pathology. Journal of Medical Imaging, 2017, 4, 021101.	1.5	2
383	Artificial Intelligence in Surveillance of Barrett's Esophagus. Cancer Research, 2021, 81, 3446-3448.	0.9	2
384	Special issue on computational pathology: An overview. Medical Image Analysis, 2021, 73, 102151.	11.6	2
385	A comparative analysis of sensitivity of convolutional neural networks for histopathology image classification in breast cancer. , 2018, , .		2
386	Radiogenomic characterization of response to chemo-radiation therapy in glioblastoma is associated with PI3K/AKT/mTOR and apoptosis signaling pathways. , 2019, , .		2
387	Computerized histomorphometric features of glandular architecture predict risk of biochemical recurrence following radical prostatectomy: A multisite study Journal of Clinical Oncology, 2019, 37, 5060-5060.	1.6	2
388	Aggregated Distance Metric Learning (ADM) for Image Classification in Presence of Limited Training Data. Lecture Notes in Computer Science, 2011, 14, 33-40.	1.3	2
389	New Radiomic Markers of Pulmonary Vein Morphology Associated With Post-Ablation Recurrence of Atrial Fibrillation. IEEE Journal of Translational Engineering in Health and Medicine, 2022, 10, 1-9.	3.7	2
390	Computational Imaging Biomarker Correlation with Intraocular Cytokine Expression in Diabetic Macular Edema. Ophthalmology Science, 2022, 2, 100123.	2.5	2
391	Combined Radiomic and Visual Assessment for Improved Detection of Lung Adenocarcinoma Invasiveness on Computed Tomography Scans: A Multi-Institutional Study. Frontiers in Oncology, 0, 12,	2.8	2
392	The interplay between intensity standardization and field inhomogeneity correction in MR image processing. , 2003, , .		1
393	MICRORNA EXPRESSION PROFILE IN CLEAR-CELL KIDNEY CANCER. Journal of Urology, 2008, 179, 92-92.	0.4	1
394	A meta-classifier for detecting prostate cancer by quantitative integration of in vivo magnetic resonance spectroscopy and magnetic resonance imaging. Proceedings of SPIE, 2008, , .	0.8	1
395	An integrated framework for analyzing three-dimensional shape differences: Evaluating prostate morphometry. , 2010, , .		1
396	Computer-assisted targeted therapy (CATT) for prostate radiotherapy planning by fusion of CT and MRI.		1

Computer , 2010, , .

ANANT MADABHUSHI

#	Article	IF	CITATIONS
397	Medial axis based statistical shape model (MASSM): Applications to 3D prostate segmentation on MRI. , 2011, , .		1
398	Linked statistical shape models for multi-modal segmentation: application to prostate CT-MR segmentation in radiotherapy planning. Proceedings of SPIE, 2011, , .	0.8	1
399	Out-of-sample extrapolation using semi-supervised manifold learning (OSE-SSL): Content-based image retrieval for prostate histology grading. , 2011, , .		1
400	Boosted Spectral Embedding (BoSE): Applications to content-based image retrieval of histopathology. , 2011, , .		1
401	Editorial: TBME Letters Special Section on Multiscale Biomedical Signal and Image Modeling and Analysis. IEEE Transactions on Biomedical Engineering, 2012, 59, 4-7.	4.2	1
402	Mouse lung volume reconstruction from efficient groupwise registration of individual histological slices with natural gradient. Proceedings of SPIE, 2013, , .	0.8	1
403	A novel point-based nonrigid image registration scheme based on learning optimal landmark configurations. , 2013, , .		1
404	Spectral embedding-based registration (SERg) for multimodal fusion of prostate histology and MRI. , 2014, , .		1
405	A statistical deformation model based regularizer for registration of histology and MRI. , 2014, , .		1
406	Front Matter: Volume 9420. , 2015, , .		1
407	Association of computerized texture features on MRI with early treatment response following laser ablation for neuropathic cancer pain: preliminary findings. Journal of Medical Imaging, 2015, 2, 041008.	1.5	1
408	The revolving door for AI and pathologists—docendo discimus?. Journal of Medical Artificial Intelligence, 2019, 2, 12-12.	1.1	1
409	Can Tumor Location on Pre-treatment MRI Predict Likelihood of Pseudo-Progression vs. Tumor Recurrence in Glioblastoma?—A Feasibility Study. Frontiers in Computational Neuroscience, 2020, 14, 563439.	2.1	1
410	SPARTA: An Integrated Stability, Discriminability, and Sparsity Based Radiomic Feature Selection Approach. Lecture Notes in Computer Science, 2021, , 445-455.	1.3	1
411	Combination of quantitative features from H&E biopsies and CT scans predicts response to chemotherapy and overall survival in small cell lung cancer (SCLC) Journal of Clinical Oncology, 2021, 39, 8572-8572.	1.6	1
412	Selecting Features with Group-Sparse Nonnegative Supervised Canonical Correlation Analysis: Multimodal Prostate Cancer Prognosis. Lecture Notes in Computer Science, 2014, 17, 385-392.	1.3	1
413	Radiomics of the lesion habitat on pre-treatment MRI predicts response to chemo-radiation therapy in Glioblastoma. , 2019, , .		1
414	ADVANCES IN COMPUTERIZED IMAGE ANALYSIS METHODS ON BREAST ULTRASOUND. , 2005, , 119-150.		1

24

#	Article	IF	CITATIONS
415	Predicting neo-adjuvant chemotherapy response from pre-treatment breast MRI using machine learning and HER2 status Journal of Clinical Oncology, 2018, 36, 582-582.	1.6	1
416	Association of radiomic features from prostate bi-parametric MRI with Decipher risk categories to predict risk for biochemical recurrence post-prostatectomy Journal of Clinical Oncology, 2019, 37, e16561-e16561.	1.6	1
417	Use of quantitative histomorphometrics to classify disease progression in HPV-positive squamous cell carcinoma Journal of Clinical Oncology, 2012, 30, 73-73.	1.6	1
418	STructural Rectal Atlas Deformation (StRAD) Features for Characterizing Intra- and Peri-wall Chemoradiation Response on MRI. Lecture Notes in Computer Science, 2019, , 611-619.	1.3	1
419	Deformation heterogeneity radiomics to predict molecular subtypes of pediatric Medulloblastoma on routine MRI. , 2019, , .		1
420	Phenotyping tumor infiltrating lymphocytes (PhenoTIL) on H&E tissue images: predicting recurrence in lung cancer. , 2019, , .		1
421	Radiomics risk score (RRS) on CT to predict survival and response to CDK 4/6 inhibitors in hormone receptor (HR) positive metastatic breast cancer (MBC) Journal of Clinical Oncology, 2020, 38, e13041-e13041.	1.6	1
422	Quantitative Nuclear Histomorphometry Predicts Molecular Subtype and Clinical Outcome in Medulloblastomas: Preliminary Findings. Journal of Pathology Informatics, 2022, 13, 100090.	1.7	1
423	Novel Imaging Biomarkers to Assess Oncologic Treatment–Related Changes. American Society of Clinical Oncology Educational Book / ASCO American Society of Clinical Oncology Meeting, 2022, , 687-699.	3.8	1
424	Generalized ball-scale: theory, algorithms, and application to image inhomogeneity correction. , 2005, 5747, 1509.		0
425	Incorporating the whole-mount prostate histology reconstruction program Histostitcher into the extensible imaging platform (XIP) framework. , 2012, , .		0
426	Learning based fiducial driven registration (LEFIR): Evaluating laser ablation changes for neurological applications. , 2013, , .		0
427	lterative multiple reference tissue method for estimating pharmacokinetic parameters on prostate DCE MRI. Proceedings of SPIE, 2013, , .	0.8	0
428	Front Matter: Volume 9041. , 2014, , .		0
429	Histomorphometry of Digital Pathology: Case Study in Prostate Cancer. , 2014, , 301-325.		Ο
430	A prostate MRI atlas of biochemical failures following cancer treatment. Proceedings of SPIE, 2014, , .	0.8	0
431	Spatially aware expectation maximization (SpAEM): application to prostate TRUS segmentation. Proceedings of SPIE, 2014, , .	0.8	0
432	Distinguishing benign confounding treatment changes from residual prostate cancer on MRI following laser ablation. Proceedings of SPIE, 2014, , .	0.8	0

#	Article	IF	CITATIONS
433	MP1-15 QUANTITATIVE HISTOMORPHOMETRIC ANALYSIS OF PROSTATE BIOPSY IMAGES PREDICT FAVORABLE OUTCOME IN ACTIVE SURVEILLANCE PATIENTS. Journal of Urology, 2015, 193, .	0.4	0
434	MP6-18 PROSTATE CANCER RECURRENCE CAN BE PREDICTED BY MEASURING NUCLEAR ORGANIZATION AND SHAPE PARAMETERS IN ADJACENT BENIGN REGIONS ON RADICAL PROSTATECTOMY SPECIMENS. Journal of Urology, 2015, 193, .	0.4	0
435	NIMG-51. IMPACT ON REMOTE FUNCTIONAL AREAS DUE TO TUMOR MASS EFFECT IS PROGNOSTIC OF OVERALL SURVIVAL IN GLIOBLASTOMA MULTIFORME. Neuro-Oncology, 2016, 18, vi135-vi135.	1.2	Ο
436	MP02-17 COMPUTER EXTRACTED NUCLEAR FEATURES FROM FEULGEN AND H&E IMAGES PREDICT BIOCHEMICAL RECURRENCE IN PROSTATE CANCER PATIENTS FOLLOWING RADICAL PROSTATECTOMY. Journal of Urology, 2016, 195, .	0.4	0
437	<i>Reply:</i> . American Journal of Neuroradiology, 2017, 38, E22-E22.	2.4	0
438	<i>Reply:</i> . American Journal of Neuroradiology, 2017, 38, E20-E20.	2.4	0
439	PD33-02 PROSTATE CANCER AGGRESSIVENESS IS MEDIATED BY AKT AND NF-ήB SIGNALING PATHWAYS: A SYSTEMS BIOLOGY APPROACH. Journal of Urology, 2017, 197, .	0.4	0
440	PD65-08 DISTINGUISHING LOW VERSUS HIGH RISK PROSTATE CANCER LESIONS USING RADIOMIC FEATURES DERIVED FROM MULTI-PARAMETRIC MAGNETIC RESONANCE IMAGING (MRI). Journal of Urology, 2017, 197, .	0.4	0
441	Reply:. American Journal of Neuroradiology, 2017, 38, E94-E94.	2.4	0
442	Deep Learning-Based Cancer Region Segmentation from H&E Slides for HPV-Related Oropharyngeal Squamous Cell Carcinomas. , 2021, , 137-147.		0
443	LuMiRa: An Integrated Lung Deformation Atlas and 3D-CNN Model ofÂInfiltrates for COVID-19 Prognosis. Lecture Notes in Computer Science, 2021, , 367-377.	1.3	0
444	Image analysis in drug discovery. , 2021, , 159-189.		0
445	Amyloid Deposition Is Greater in Cerebral Gyri than in Cerebral Sulci with Worsening Clinical Diagnosis Across the Alzheimer's Disease Spectrum. Journal of Alzheimer's Disease, 2021, 83, 423-433.	2.6	0
446	Tissue mechanics during acupuncture and manual therapies. FASEB Journal, 2007, 21, A84.	0.5	0
447	Nonâ€invasive theranostic to predict and assess response to atherosclerotic drugs. FASEB Journal, 2013, 27, 686.4.	0.5	0
448	Abstract 4352: Prediction of prostate cancer progression with biomarkers and tissue morphometry changes. , 2015, , .		0
449	Abstract 4349: Cancer histologic and cell nucleus architecture differentiate prostate cancer Gleason patterns 3 from 4. , 2015, , .		0
450	Computer extracted nuclear features from Feulgen and H&E images to predict biochemical recurrence in prostate cancer patients following radical prostatectomy Journal of Clinical Oncology, 2016, 34, 5067-5067.	1.6	0

#	Article	IF	CITATIONS
451	Computerized textural analysis of DCE-MRI to enable identification of HER2-enriched breast cancers Journal of Clinical Oncology, 2016, 34, 598-598.	1.6	0
452	Computer extracted features on H&E images to improve biochemical recurrence prediction of Kattan nomogram for prostate cancer patients following radical prostatectomy: Preliminary findings Journal of Clinical Oncology, 2016, 34, 11556-11556.	1.6	0
453	Computer extracted measurements of intra-tumoral heterogeneity on H&E stained tissue images to distinguish short term and long term survivors in patients with non-small cell lung carcinoma Journal of Clinical Oncology, 2017, 35, e20052-e20052.	1.6	0
454	Computer extracted features of nuclear architecture in H&E sections to predict disease recurrence in oropharyngeal squamous cell carcinoma patients Journal of Clinical Oncology, 2017, 35, e17536-e17536.	1.6	0
455	Computer extracted shape features of prostate capsule from MRI to predict biochemical recurrence of prostate cancer post-treatment Journal of Clinical Oncology, 2017, 35, e16579-e16579.	1.6	0
456	Computer extracted measurements of vessel tortuosity on baseline CT scans to predict response to nivolumab immunotherapy for non-small cell lung cancer Journal of Clinical Oncology, 2017, 35, 11566-11566.	1.6	0
457	Computer extracted nuclear features from tumor and benign regions of Feulgen and H&E images to help predict recurrence in prostate cancer patients following radical prostatectomy Journal of Clinical Oncology, 2017, 35, e16556-e16556.	1.6	0
458	A combination of computer extracted measurements of prostate capsule shape and tumor texture on MRI to predict biochemical recurrence post treatment Journal of Clinical Oncology, 2017, 35, e16554-e16554.	1.6	0
459	Computer extracted features of gland morphology on H&E surgically resected tissue images as predictive of biochemical recurrence and rate of expression in African American compared to Caucasian American men Journal of Clinical Oncology, 2017, 35, e16559-e16559.	1.6	0
460	Abstract 1080: Targeting the PI3K-Akt and NF-κB pathways as a combination therapy in blocking prostate cancer progression. , 2017, , .		0
461	A lymphocyte spatial distribution graph-based method for automated classification of recurrence risk on lung cancer images. , 2017, , .		0
462	Quantifying expert diagnosis variability when grading tumor-infiltrating lymphocytes. , 2017, , .		0
463	Combination of nuclear NF-kB/p65 localization and gland morphological features from surgical specimens appears to be predictive of early biochemical recurrence in prostate cancer patients. , 2018, , .		0
464	Combination of CT derived radiomic features and lymphovascular invasion status to predict disease recurrence following trimodality therapy in non-small cell lung cancer Journal of Clinical Oncology, 2018, 36, e24314-e24314.	1.6	0
465	Abstract LB-021: Combination of quantitative histomorphometry with NFκB/p65 nuclear localization is better predictor of biochemical recurrence in prostate cancer patients. , 2018, , .		0
466	Integrating radiomic features from T2-weighted and contrast-enhanced MRI to evaluate pathologic rectal tumor regression after chemoradiation. , 2019, , .		0
467	Radiomic characterization of perirectal fat on MRI enables accurate assessment of tumor regression and lymph node metastasis in rectal cancers after chemoradiation. , 2019, , .		0
468	Spatial arrangement of leakage patterns in diabetic macular edema is associated with tolerance of aflibercept treatment interval length: preliminary findings. , 2019, , .		0

#	Article	IF	CITATIONS
469	Radiomic features derived from pre-operative multi-parametric MRI of prostate cancer are associated with Decipher risk score. , 2019, , .		0
470	Morphology of vascular network in eyes with diabetic macular edema varies based on tolerance of aflibercept treatment interval length: preliminary findings. , 2019, , .		0
471	Intra and perinodular CT delta radiomic features associated with early response to predict overall survival (OS) in immunotherapy-treated non-small cell lung cancer (NSCLC): A multisite multi-agent study Journal of Clinical Oncology, 2019, 37, 2588-2588.	1.6	0
472	Radiomics in genitourinary cancers. , 2019, , 301-317.		0
473	History of the SPIE Medical Imaging Digital Pathology Conference. Journal of Medical Imaging, 2022, 9, 012203.	1.5	0
474	Identifying the origination of liver metastasis using a hand-crafted computational pathology approach. , 2022, , .		0
475	Computer extracted features of tumor-infiltrating lymphocytes (TILs) architecture are prognostic of progression-free survival in stage III colon cancer. , 2022, , .		0
476	Response to: Correspondence on 'Novel imaging biomarkers predict outcomes in stage III unresectable non-small cell lung cancer treated with chemoradiation and durvalumab' by Zheng <i>et al</i> , 2022, 10, e005086.		0
477	Fifty years of SPIE Medical Imaging proceedings papers. Journal of Medical Imaging, 2022, 9, .	1.5	0